Journal of Biomedical Optics

BiomedicalOptics.SPIEDigitalLibrary.org

Identification of kidney tumor tissue by infrared spectroscopy of extracellular matrix

Vidita Urboniene
Milda Pucetaite
Feliksas Jankevicius
Arunas Zelvys
Valdas Sablinskas
Gerald Steiner

SPIE.

Identification of kidney tumor tissue by infrared spectroscopy of extracellular matrix

Vidita Urboniene,[a] Milda Pucetaite,[a] Feliksas Jankevicius,[b] Arunas Zelvys,[b] Valdas Sablinskas,[a,*] and Gerald Steiner[a,c]
[a]Vilnius University, Department of General Physics and Spectroscopy, Sauletekio av. 9 bl. 3, Vilnius, LT-10234, Lithuania
[b]Vilnius University, Urology Center, Santariskiu Str. 2, LT-08661 Vilnius, Lithuania
[c]Technische Universität Dresden, Medizinische Fakultät Carl Gustav Carus, Klinisches Sensoring und Monitoring, Fetscher Str. 74, 01307 Dresden, Germany

Abstract. Fourier transform infrared (FT-IR) spectroscopy was applied to characterize the extracellular matrix (ECM) of kidney tumor tissue and normal kidney tissue. Freshly resected tissue samples from 31 patients were pressed on a CaF_2 substrate. FT-IR spectra obtained from ECM of tumor tissue exhibit stronger absorption bands in the spectral region from 1000 to 1200 cm^{-1} and around 1750 cm^{-1} than those obtained from normal tissue. It is likely that the spectra of ECM of kidney tumor tissue with large increases in the intensities of these bands represent a higher concentration of fatty acids and glycerol. Amide I and amide II bands are stronger in the spectra of ECM from normal tissue, indicating a higher level of proteins. Our results suggest that FT-IR spectroscopy of the ECM is an innovative emerging technology for real-time intraoperative tumor diagnosis, which may improve margin clearance in renal cancer surgery. [DOI: 10.1117/1.JBO.19.8.087005]

Keywords: Fourier transform infrared spectroscopy; kidney tumor; extracellular matrix.

Paper 140251PR received Apr. 20, 2014; revised manuscript received Jul. 8, 2014; accepted for publication Jul. 17, 2014; published online Aug. 20, 2014.

1 Introduction

Renal cell carcinoma (RCC), the most common type of kidney cancer, is increasing in incidence and is the most lethal genitourinary cancer.[1] Surgical resection of RCC is the benchmark for long-term cure of this disease. In recent years, enhanced employment of different imaging techniques has increased the number of patients with small renal tumors. Nephron-sparing surgery is the preferred operative modality for small renal masses because it offers equivalent oncologic efficacy and improved renal function outcomes compared with complete nephrectomy.[2] Additionally, minimally invasive surgical approaches, including laparoscopic and robot-assisted partial kidney resection, have become more and more popular due to better cosmetic results and faster recovery compared with open operations. Despite the advantages of nephron-sparing resections, the surgical technique is difficult to perform and has a steep learning curve.

Preoperative diagnostic examinations by computer tomography or magnetic resonance imaging and ultrasound provide borders for the safe tumor resection. However, intraoperative detection of tumor margins is challenging and, up till now, is merely based on palpation and visual inspection, resulting, frequently, in incomplete tumor resection. Intraoperative rapid pathological microscopic examination, known as a frozen section procedure, is time consuming, is of lower quality than fixed tissue processing, highly depends on the investigator's skills, and may be unreliable.[3] Therefore, rapid and reliable technology for intraoperative identification of cancer cells is urgently needed for tumor margin controlled surgery.

Recently, several attempts have been made to apply bioanalytical methods for an intraoperative classification of tissue. In particular, vibrational spectroscopy has the potential for identification of tumor cells under intraoperative conditions.[4]

During the last decades, many studies have demonstrated that Fourier transform infrared (FT-IR) spectroscopy is a tool for quick and label-free characterization of biological materials.[5–10] FT-IR spectroscopy can be used to detect very small variations in spectral fingerprints. Different techniques are applied for diagnosis of tissue pathologies:[11] IR microspectroscopy,[6,8,9] Raman spectroscopy, and fluorescence spectroscopy.[12] FT-IR and Raman spectroscopic techniques have been applied to a broad spectrum of biochemical samples, such as thyroid gland,[13] brain, and even the primary tumor of brain metastases,[14,15] breast,[16] skin, and cervical cancer,[17] and many others, such as prostate, stomach, kidney, and lung tumors.

The majority of these studies are based on the investigation of cells.[18,19] Recent evidence indicates that tumor cells interact through direct cell–cell as well as cell–matrix interactions controlled by the production of specific extracellular matrix (ECM) components and the secretion of grow factors.[20] It is well known that the ECM plays an important role in sustaining tissue cells and alterations may indicate the transformation of normal tissue into tumor tissue. Of the many available techniques for characterization of ECM, FT-IR spectroscopy is gaining attention as it provides label-free insights into the molecular composition.[21–23] For example, glioma cells are known to produce an ECM-like chemical fingerprint,[24] which can be detected by FT-IR spectroscopy.[25]

*Address all correspondence to: Valdas Sablinskas, E-mail: valdas.sablinskas@ff.vu.lt

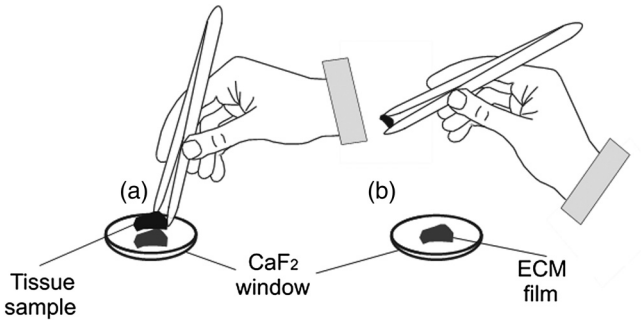

Fig. 1 Scheme of the sample preparation procedure. (a) The freshly resected tissue is placed on the CaF_2 slide. (b) An extracellular matrix (ECM) film remains on the substrate after removing the tissue.

In this study, we demonstrate that FT-IR spectroscopy can be used for an analysis of ECM to classify normal and tumor kidney tissue.

2 Experimental

2.1 *Sample Preparation*

The samples for FT-IR spectroscopic studies were prepared from freshly resected human kidney tissue. Tumor and control specimens were obtained from 31 adult patients, who underwent kidney tumor surgery at the Urology Department of Vilnius University (9 female, 22 male, with an age of 42 to 83 years). The protocol of this study was approved by the Vilnius regional bioethics committee (approval no. 158200-12-131-056LP6, 05 05 2009). Figure 1 illustrates the preparation of ECM films graphically. A small volume of freshly resected tissue is deposited on CaF_2 slide and removed after a few seconds. ECM on the slide was dried at room temperature.

2.2 *FT-IR Spectroscopic Imaging*

FT-IR spectroscopic imaging was performed in transmission mode using an FT-IR spectrometer Vertex 70 coupled with an infrared microscope Hyperion 3000 (both from BrukerOptik GmbH, Ettlingen, Germany) and a mercury cadmium telluride (MCT) focal plane 64×64 array detector. The 15-fold Cassegrainian objective with a numerical aperture of 0.4 imaged a sample area of $\sim 175 \times 175\ \mu m^2$. Composition of individual infrared images was captured. Pixel binning of 4×4 was applied for the larger composition in order to reduce the amount of spectra. Pixel binning reduces the lateral resolution to $\sim 22\ \mu m [=> 2 \times (175\ \mu m/64\ \text{pixel} \times \text{binning}\, 4)]$. The background spectroscopic image was recorded before the ECM films were investigated from the pure CaF_2 window. A total number of 16 interferograms (scans) were co-added. The interferograms were Fourier transformed applying Blackman–Harris 3-Term apodization and a zero filling factor of 2. Spectra at a resolution of 8 cm^{-1} of the sample image were ratioed against the spectra of the background image and transformed to absorbance values. This spectral resolution was chosen in order to improve the signal-to-noise ratio, to reduce the size of the spectral data set, and to ensure that all prominent bands, even those with medium intensity, appear clearly in the spectrum.

2.3 *FT-IR Microspectroscopy*

For each sample, FT- IR spectra were acquired using the Vertex 70 instrument coupled with an infrared microscope Hyperion 3000 and a single-point MCT detector. The aperture size was set to $100 \times 100\ \mu m^2$. One hundred and twenty eight interferograms were recorded at a resolution of 4 cm^{-1}, apodized (Blackman–Harris 3-Term), zero filled (two times), and phase corrected (Mertz). After Fourier transformation, the single-beam sample spectra were ratioed against a background spectrum obtained from the pure CaF_2 window and converted to absorbance units.

2.4 *Data Evaluation*

Evaluation of all spectral data was performed using the MATLAB® Package (Version 7, Math Works Inc., Natick, Massachusetts). The so-called fingerprint region between 950 and 1800 cm^{-1} was considered. Data preprocessing for both spectroscopic image and single-point measurements involves the removal of outliers, a baseline correction, and a normalization of each absorbance value of a spectrum to the integral absorbance. Outliers are spectra that are obviously not associated to tissue or spectra with a maximum absorbance value >1.8 or <0.05. The baseline of each spectrum was corrected by using the *msbackadj* function of the Statistics Toolbox of the MATLAB® package. Afterward, the spectra were area-normalized to eradicate spectral differences due to sample thickness or variation in the density of cellulose fibers. The *eig* function of the basic MATLAB® package was used for principal component analysis (PCA) calculation of the spectroscopic image.

3 Results

Figure 2 shows the hematoxylin and eosin (H&E) stain for a section of renal tumor tissue, adjacent to a piece that was used for preparation of ECM. The H&E section shows areas of different cellular density and structure as well as necrotic tissue. Small dark blue dots evenly distributed in the H&E image represent the nuclei of tumor cells. Such features are associated with an undifferentiated type of RCC.

In a first experimental step, FT-IR imaging was used to quantitatively investigate the homogeneity of the prepared ECM films. The objective of this initial study was to examine whether single-point measurements of ECM films are meaningful to distinguish between normal and tumor samples. Figure 3(a) shows

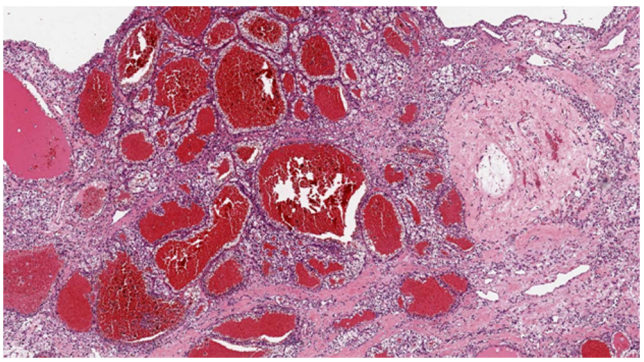

Fig. 2 Hematoxylin and eosin stain of undifferentiated type of renal cell carcinoma. The image has a dimension of $4.0 \times 2.0\ mm^2$.

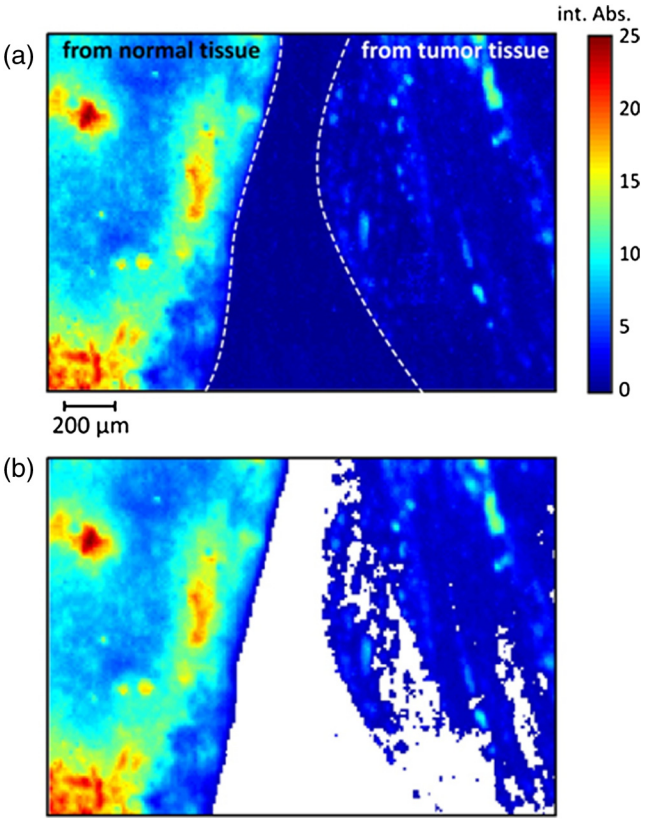

Fig. 3 (a) Fourier transform infrared (FT-IR) imaging of ECM films. The image contrast is calculated by the integrated absorbance between 950 and 1800 cm^{-1}. (b) The corrected image, where areas with no sample appear as white pixels.

the FT-IR image of the raw data set. Normal tissue was pressed on the left side and tumor tissue on the right side of the CaF_2 window.

All absorbance values in the range from 950 to 1800 cm^{-1} of each individual spectrum are summarized and color-coded in the rainbow scale. Baseline correction was applied to the absorbance spectra. Spectra that obviously do not correspond to the ECM film are detected as outliers and were removed from the data set. Figure 3(b) shows the FT-IR image of the preprocessed data set. Similar to Fig. 3(a), absorbance values are summarized and color-coded in the rainbow scale. White pixels indicate spectra that were removed from the data set. The ECM film of normal tissue exhibits stronger absorbance values than the ECM film of tumor tissue. Normal tissue is denser and less wet than tumor tissue. Consequently, after drying, the ECM film of tumor tissue is thinner than the film from normal tissue.

As the FT-IR spectroscopic imaging has generated a complex data set containing thousands of spectra, a multivariate approach has been chosen for the analysis. The investigation of the spectral signals was performed by PCA. This method is known to provide a rapid way to assess variation within the spectral data set and it assumes no explicit statistical model underlying the variance of the original spectra. Principal components (PC) are formed by loading plots and score maps. The loading plots correspond to spectral bands where the variation is the highest and weight the signals in the positive and negative directions. The score map reveals the weight of the loading plot for each pixel of the image. PCA is applied on the preprocessed spectra. Loading vectors and score maps of the first five PC are represented in Fig. 4. The first PC exhibits a variance of 91%. It represents the mean spectrum of the samples. The amide I and II bands, located at 1542 and 1650 cm^{-1},[26] respectively, are the major bands in the loading plot. The signal at ~1739 cm^{-1} arises from ν_s(C═O) modes of lipids or esters, and the signal located at 1394 cm^{-1} is assigned to $\nu_{as}(COO^-)$ of fatty acids.[26]

Additional absorption features here are due to $\delta(CH_2)$ at 1455 cm^{-1} and the amide III mode at 1237 cm^{-1}. A broad signal between 1000 and 1250 cm^{-1} is the result of the ν(C─O), ν(P─O), and ν(C─C─O) modes.[26] The score map of the second PC shows a clear difference between normal and tumor samples. Chartreuse pixels mainly indicate positive score values for the ECM film of normal tissue, whereas the ECM film of tumor tissue is dominated by green and blue pixels and negative score values. The corresponding loading plot displays three pronounced negative signals, which are assigned to ν_{as}(C─O) of esters (1164 cm^{-1}), $\delta(CH_2)$, and $\nu_{as}(COO^-)$ modes. Vibrations of fatty acids may also contribute to the signal at 1739 cm^{-1}. The signals indicate that the ECM of tumor tissue contains more esters and fatty acids than the ECM of normal tissue. It should be noted that the signal intensity between 1730 and 1750 cm^{-1} can be affected by variations of the ester content as well as by pH. A lower extracellular pH is an important feature of tumor tissue.[27] The extracellular acidification of tumor tissue is considered to be due to lactate secretion from anaerobic glycolysis.[28] An acidic pH leads to an increase of the protonated acid form and, consequently, to an enhanced signal in the aforementioned spectral range.

Three small areas of blue pixels in the ECM film of normal tissue may occur due to blood clots present in the sample of the intercellular fluid. Nevertheless, the score map clearly indicates that the ECM from both, normal and tumor tissues, form nearly homogeneous films, which allow point measurements. The third PC also shows slight differences between both types of ECMs. However, a detailed discussion of the loading plot is hardly possible. Weaker and slightly shifted signals compared to the loading plot of the second PC and, most notably, the appearance of a broad signal with a maximum at 1054 cm^{-1} as well as a weak negative amide I signal at 1664 cm^{-1} points to complex variations of biochemical composition. The fourth and higher PCs contribute only slightly to the measured variance; hence, they mainly represent noise signals without any further relevant information.

Since the PCA reveals significant spectral differences between ECM films of normal and tumor tissues as well as a comparatively homogeneous distribution of the different spectral features, further spectral analysis was performed by the faster single-point measurement mode. For each sample, five randomly chosen points were measured and then averaged. This reduces variations in the spectra due to inhomogeneities of the ECM. Figure 5(a) shows the mean spectra of the ECM films prepared from normal tissue. Although the overall absorbances fluctuate from sample to sample, the spectral pattern is very similar. This becomes much more pronounced when the spectra are area normalized, as shown in Fig. 5(b). Shown in Figs. 5(c) and 5(d) are the raw and normalized spectra of ECM films from tumor tissue. All the tumor ECM films exhibit a stronger signal between 1730 and 1750 cm^{-1}, which arises from carbonyl groups of fatty acids. The broad signal between 1000 and 1200 cm^{-1} is dramatically altered as well, splitting into several separate bands at ~1050, 1080, and 1150 cm^{-1}.

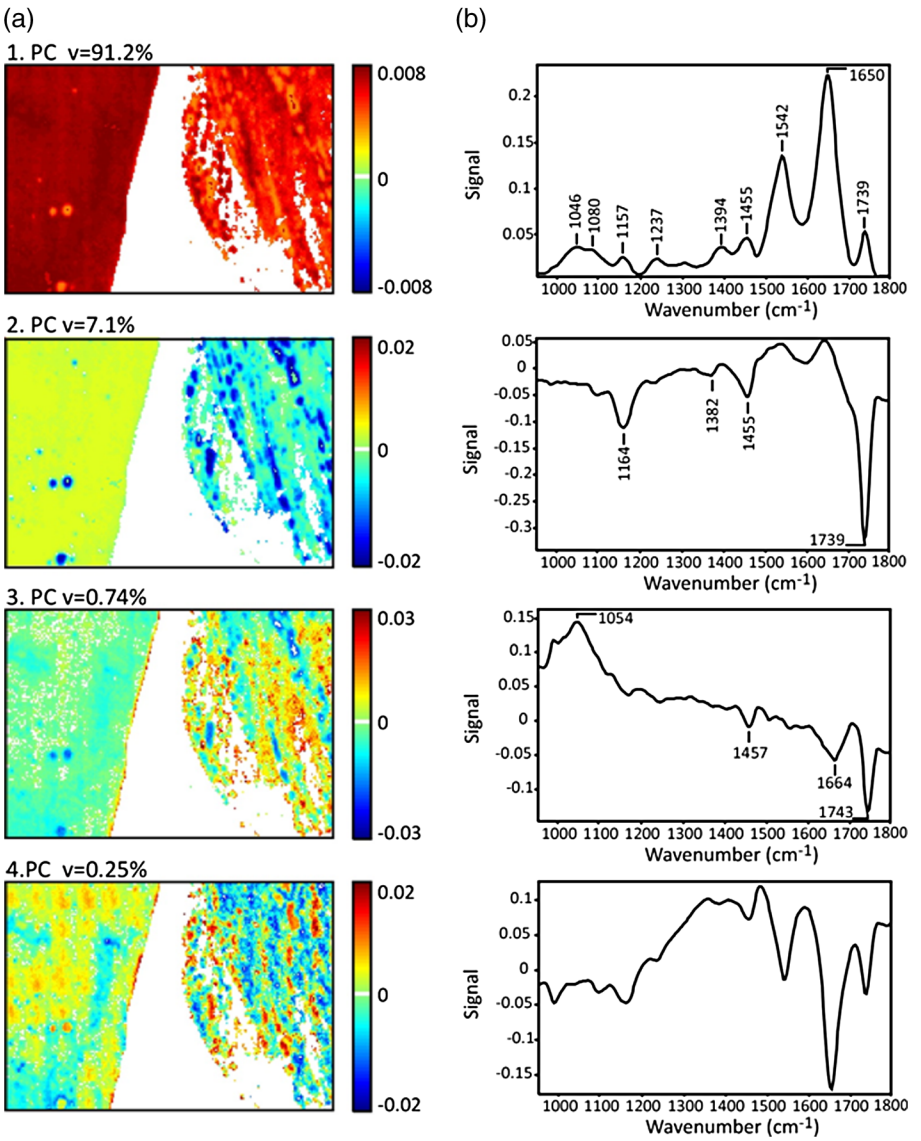

Fig. 4 Principal component analysis of the selected spectra. (a) Score maps and (b) corresponding loading plots.

These bands are known to be due to carbohydrates, phosphate groups, and glycolipids, which, in the tumor samples, have a weak but discernible increase in absorption. This finding is supported by a recently published Raman spectroscopic study which shows that kidney tumor tissue exhibits increased phosphate stretching modes.[29] Obviously, the carbonyl stretching band, centered at 1750 cm^{-1}, and the broad signal between 1000 and 1200 cm^{-1} can both be used as spectral markers to distinguish the ECM of tumor from those of normal tissue. The ECM of tumor tissue exhibits a significantly higher content of fatty acids, carbohydrates, phosphate groups, and glycolipids than the ECM of a normal sample. This general trend is observed for all 31 patients. The scatter plot of the integrated intensity between 1000 and 1200 cm^{-1} versus the integrated intensity between 1710 and 1780 cm^{-1} is depicted in Fig. 6.

The variance for the ECM of tumor tissue is higher than the ECM of normal tissue. Tumor tissue varies significantly between individuals, as expected. RCC and urothelial cell carcinoma are known for displaying a high amount of interindividual variance.

The absorbance values corresponding to the ECM of normal and tumor tissues can be precisely separated by two defined thresholds as indicted in Fig. 6. Spectra that have an integrated absorbance >0.013 in the spectral range from 1710 to 1780 cm^{-1} and a higher integrated absorbance of 0.07 in the range from 1000 to 1200 cm^{-1} are classified as tumor.

The ECM sample, marked with a star in the plot, exhibits a much higher intensity of the carbonyl band than that of the other ECM samples of normal tissue. A detailed inspection of this ECM film indicated very low absorbance values and, consequently, a low signal-to-noise ratio. This led, obviously, to a calculated stronger intensity of the carbonyl band. Low absorbance values can be explained by the very low thickness of the dried film, produced by not applying enough pressure during the stamping of the tissue on the substrate.

For the first time, we have demonstrated an optical marker-free technology to identify kidney tumor tissue. Although

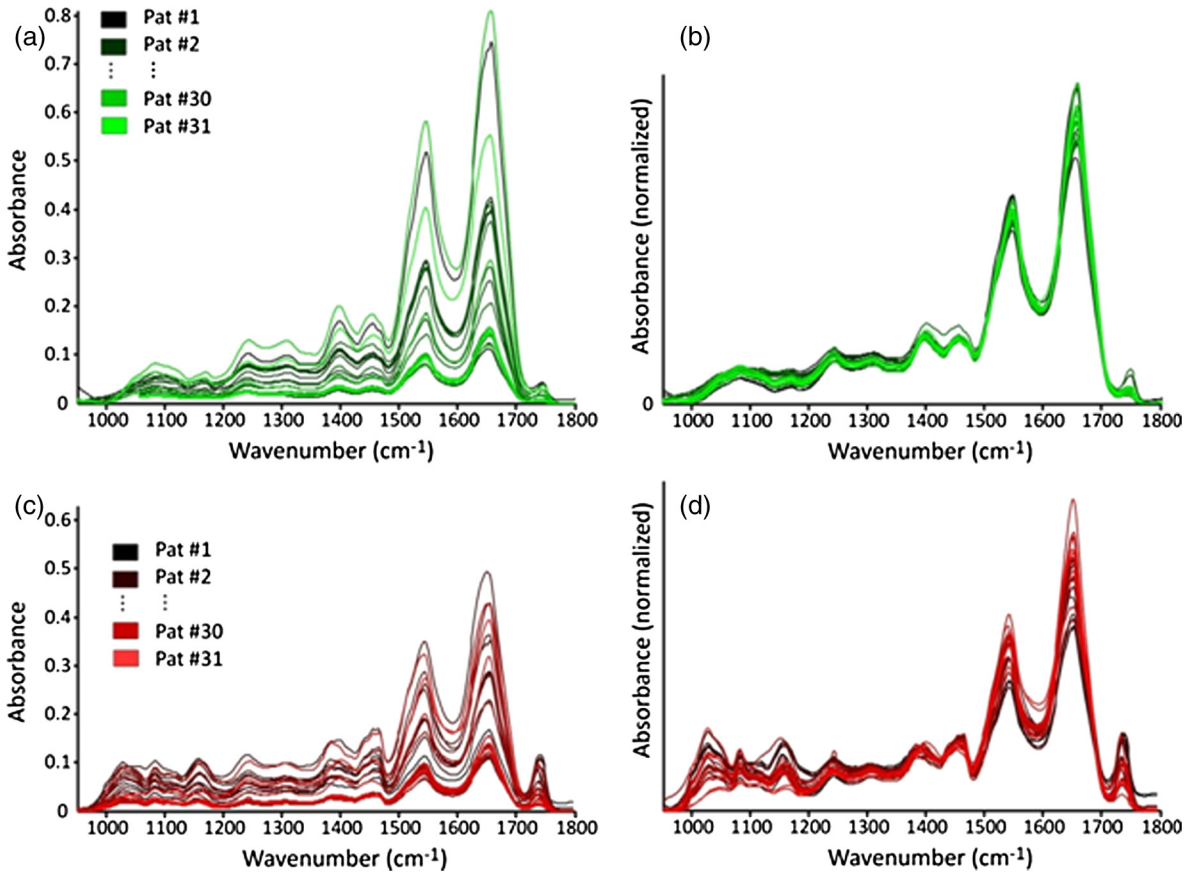

Fig. 5 FT-IR spectra of ECM films obtained from 31 cases. (a) Baseline-corrected raw spectra obtained from normal tissue and (b) spectra after area normalization. (c) Corresponding baseline-corrected raw spectra obtained from tumor tissue and (d) spectral area normalized.

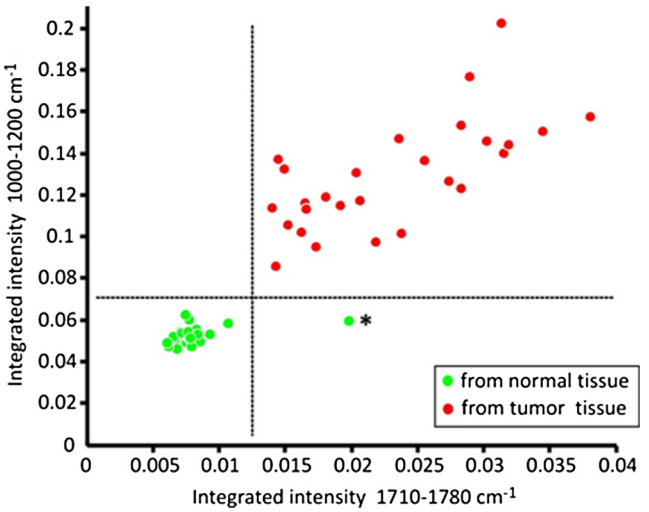

Fig. 6 Integrated intensity between 1000 and 1200 cm^{-1} versus 1710 and 1780 cm^{-1} of ECM spectra from 31 cases. The dotted lines indicate thresholds to distinguish between both types of tissue. One case of ECM obtained from normal tissue exhibits a higher integrated intensity of the carbonyl band (marked by a star); for details, see the text.

intraoperative FT-IR spectroscopy is still far from clinical routine applications, this study demonstrates that freshly resected tissue can be analyzed quickly and accurately to obtain diagnostic information in the operating room. Moreover, the evaluation of ECM enables an intraoperative analysis of questionable tissue without surgical resection.

4 Conclusions

In this article, we demonstrate that FT-IR spectroscopy based on the characterization of ECM is useful for a label-free differentiation of kidney tumor from normal tissue. Reproducible differences are apparent between spectra of tumor and normal ECM in the C=O stretching region (1710 to 1780 cm^{-1}) and in the range between 1000 and 1200 cm^{-1}. These spectral regions can be used as markers for the identification of the presence of the tumor cells in tissue. Importantly, FT-IR spectroscopy, in particular, makes possible a label-free and rapid assessment of questionable kidney tissue during the operative resection of the tumor. Larger prospective studies are needed to confirm these preliminary data.

Acknowledgments

Funding from the European Community's social foundation under Grant Agreement No. VP1-3.1-ŠMM-08-K-01-004/KS-120000-1756 is acknowledged.

References

1. J. N. Eble et al., *Pathology and Genetics of Tumors of the Urinary System and Male Genital Organs*, World Health Organization (2004).
2. M. Crepel et al., "Nephron-sparing surgery is equally effective to radical nephrectomy for T1BN0M0 renal cell carcinoma: a population-based assessment," *Urology* **75**(2), 271–275 (2010).
3. S. Venigalla, G. Wu, and H. Miyamoto, "The impact of frozen section analysis during partial nephrectomy on surgical margin status and tumor recurrence: a clinicopathologic study of 433 cases," *Clin. Genitourin Cancer* **11**(4), 527–536 (2013).
4. G. Steiner and M. Kirsch, "Optical spectroscopic methods for intraoperative diagnosis," *Anal. Bioanal. Chem.* **406**(1), 21–25 (2014).
5. R. K. Sahu and S. Mordechai, "Fourier transform infrared spectroscopy in cancer detection," *Future Oncol.* **1**(5), 635–647 (2005).
6. G. Srinivasan and R. Bhargava, "Fourier transform–infrared spectroscopic imaging: the emerging evolution from a microscopy tool to a cancer imaging modality," *Spectroscopy* **22**(7), 40–51 (2007).
7. B. R. Wood et al., "An investigation into FTIR spectroscopy as biodiagnostic tool for cervical cancer," *Biospectroscopy.* **2**(3), 143–153 (1996).
8. B. R. Wood et al., "Fourier transform infrared (FTIR) spectral mapping of the cervical transformation zone, and dysplastic squamous epithelium," *Gynecol. Oncol.* **93**(1), 59–68 (2004).
9. I. W. Levin and R. Bhargava, "Fourier transform infrared vibrational spectroscopic imaging: integrating microscopy and molecular recognition," *Annu. Rev. Phys. Chem.* **56**, 429–474 (2005).
10. R. K. Dukor, "Vibrational spectroscopy in the detection of cancer," in *The Handbook of Vibrational Spectroscopy*, J. M. Chalmers and P. R. Griffiths, Eds., pp. 3335–3361, John Wiley & Sons Ltd., Chichester (2002).
11. C. Krafft et al., "Disease recognition by infrared and Raman spectroscopy," *J. Biophotonics* **2**(1–2), 13–28 (2009).
12. R. Manoharan et al., "Raman spectroscopy and fluorescence photon migration for breast cancer diagnosis and imaging," *Photochem. Photobiol.* **67**(1), 15–22 (1998).
13. Y. Liu et al., "Detection of cervical metastatic lymph nodes in papillary thyroid carcinoma by Fourier transform infrared spectroscopy," *Br. J. Surg.* **98**(3), 380–394 (2011).
14. N. Bergner et al., "Tumor margin identification and prediction of the primary tumor from brain metastases using FTIR imaging and support vector machines," *Analyst* **138**(14), 3983–3990 (2013).
15. C. Krafft et al., "Identification of primary tumors of brain metastases by SIMCA classification of IR spectroscopic images," *BBA* **1758**(7), 883–891 (2006).
16. A. Benard et al., "Discrimination between healthy and tumor tissues on formalin-fixed paraffin-embedded breast cancer samples using IR imaging," *Spectroscopy* **24**(1–2), 67–72 (2010).
17. S. Mordechai, K. R. Sahu, and Z. Hammody, "Possible common biomarkers from FTIR microspectroscopy of cervical cancer and melanoma," *J. Microsc.* **215**(1), 86–91 (2004).
18. J. P. Couapel et al., "Optical spectroscopy techniques can accurately distinguish benign and malignant renal tumors," *BJU Int.* **111**(6), 865–871 (2013).
19. S. Stewart et al., "Distinguishing between renal oncocytoma and chromophobe renal carcinoma using Raman molecular imaging," *J. Raman Spectrosc.* **45**(4), 274–280 (2014).
20. C. M. Vicente et al., "Syndecan-2 is upregulated in colorectal cancer cells through interactions with extracellular matrix produced by stromal fibroblasts," *BMC Cell Biol.* **14**(25) (2013).
21. R. Noreen et al., "FTIR spectro-imaging of collagen scaffold formation during glioma tumor development," *Anal. Bioanal. Chem.* **405**(27), 8729–8736 (2013).
22. S. Kumar et al., "Change in the microenvironment of breast cancer studied by FTIR imaging," *Analyst* **138**(14), 4058–4065 (2013).
23. N. Hassler et al., "Real-time spectroscopic analysis of extracellular matrix produced by MC3T3-E1 preosteoblastic cells cultured under dynamic conditions," *Appl. Spectrosc.* **66**(1), 40–47 (2012).
24. I. A. Edwards et al., "Effect of brain-tumor derived connective tissue growth factor on glioma invasion," *J. Natl. Cancer Inst.* **103**(15), 1162–1178 (2011).
25. A. L. Stelling et al., "Infrared spectroscopic studies of cells and tissue: triple helix proteins as a potential biomarker for tumors," *PLOS One* **8**(3), 358332 (2013).
26. G. Socrates, *Infrared and Raman Characteristic Group Frequencies*, J. Wiley & Sons Ltd., West Sussex, England (2001).
27. L. E. Gerweck and K. Seetharaman, "Cellular pH gradient in tumor versus normal tissue: potential exploitation for the treatment of cancer," *Cancer Res.* **56**(6), 1194–1198 (1996).
28. Y. Kato et al., "Acidic extracellular microenvironment and cancer," *Cancer Cell Int.* **13**, 89 (2013).
29. Z. Zhengfei et al., "Study of molecule variations in renal tumors based on confocal micro-Raman spectroscopy," *J. Biomed. Opt.* **18**(3), 031103 (2013).

Biographies of the authors are not available.